

Rotational spectra of interstellar N- and CN-PAHs: pyrene and coronene

Akant Vats[★] and Amit Pathak[†]

Department of Physics, Institute of Science, Banaras Hindu University, Varanasi-221005, India

Accepted XXX. Received YYY; in original form ZZZ

ABSTRACT

The detection of benzonitrile (C_6H_5CN), 1- and 2-cyano-naphthalene ($C_{10}H_7CN$) in the cold, dark molecular cloud TMC-1 at centimetre (cm) wavelengths has opened up prospects for the detection of other N- and CN-containing polycyclic aromatic hydrocarbons (PAHs). In this light, the pure rotational spectra of N-pyrene ($C_{15}H_9N$), CN-pyrene ($C_{15}H_9CN$), N-coronene ($C_{23}H_{11}N$) and CN-coronene ($C_{23}H_{11}CN$) are reported here for the first time. The B3LYP/6-311+G(d,p) level of theory, in the Density Functional Theory (DFT) calculations, achieves the best performance for calculating the spectroscopic parameters and simulating the rotational spectra. The large permanent dipole moment of CN-PAHs makes them the most suitable PAH species for detection in the interstellar medium. Additionally, pyrene’s smaller partition function makes CN-pyrene a prime candidate to be discovered in cold, dark molecular clouds such as the TMC-1. The present work sets a benchmark for theoretical rotational spectra of N- and CN-containing PAHs and may act as a guide for laboratory experiments and observational searches.

Key words: astrochemistry – molecular processes – ISM: molecules – ISM: clouds – radio lines: ISM.

1 INTRODUCTION

The mid-infrared (IR) spectra of the interstellar medium (ISM) of our Galaxy and several other galaxies are dominated by the emission features peaking strongly at 3.3, 6.2, 7.7, 8.6, 11.2 and 12.7 μm , commonly known as unidentified infrared (UIR) bands (Gillett et al. 1973; Cohen et al. 1986; Onaka et al. 1996; Sloan et al. 1999; Peeters et al. 2002; Li 2020). The UIR bands are ubiquitous characteristics of a wide variety of astronomical sources including H II regions, post-AGB stars, young stellar objects (YSOs), planetary nebulae (PNe), reflection nebulae (RNe), the ISM of galaxies as well as the diffuse ISM (Hony et al. 2001; Verstraete et al. 2001; Peeters et al. 2002; Smith et al. 2007; Sloan et al. 2007). These bands are a result of the IR fluorescence involving the vibrational bands of polycyclic aromatic hydrocarbon (PAH) molecules after absorption of ultraviolet (UV) photons (Leger & Puget 1984; Allamandola et al. 1985, 1989; Onaka 2004; Tielens 2008). About 15% of the interstellar carbon may be associated with PAHs and related species and these PAHs affect the chemical and physical processes in their habitat (Tielens 2008; Li 2020). Other than their vibrational emission, the rotational emission from PAHs seems most appropriate carrier of “anomalous microwave emission” (AME) present in the frequency range of 10–60 GHz (Kogut et al. 1996; Leitch et al.

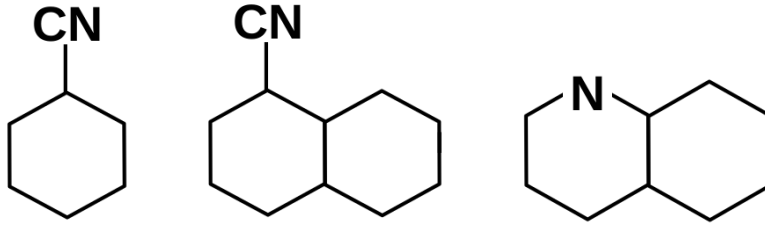
1997; Hensley et al. 2022). Furthermore, the electronic spectra of PAHs may interpret some of the diffuse interstellar bands (DIBs); absorption bands observed in the UV and optical (Salama et al. 2011).

Despite the importance of PAHs as a common and ubiquitous interstellar molecule, the detection of a specific PAH in the ISM through UIR bands is quite challenging as they arise from nearest neighbour vibrations and could be mixtures of different PAH species (Tielens 2008). On the other hand, pure rotational spectroscopy is a powerful technique in detection of the interstellar molecules and have been used to identify around 80% of molecules observed in the space (McGuire et al. 2018). Due to the lack of a permanent dipole moment in PAHs and structural similarities, this technique is not useful for PAHs. However, a bowl-shaped PAH molecule having a large permanent dipole moment, corranulene ($C_{20}H_{10}$) has been searched for using rotational spectroscopy, with no success (Pilleri et al. 2009). Later on, it has been found that planar molecules such as PAHs can have a permanent dipole moment if they carry some impurity, mainly in the form of substitution or having different side groups (Ali-Haïmoud 2014). This marks a silver-lining about the brighter prospects of rotational spectroscopy for interstellar PAHs.

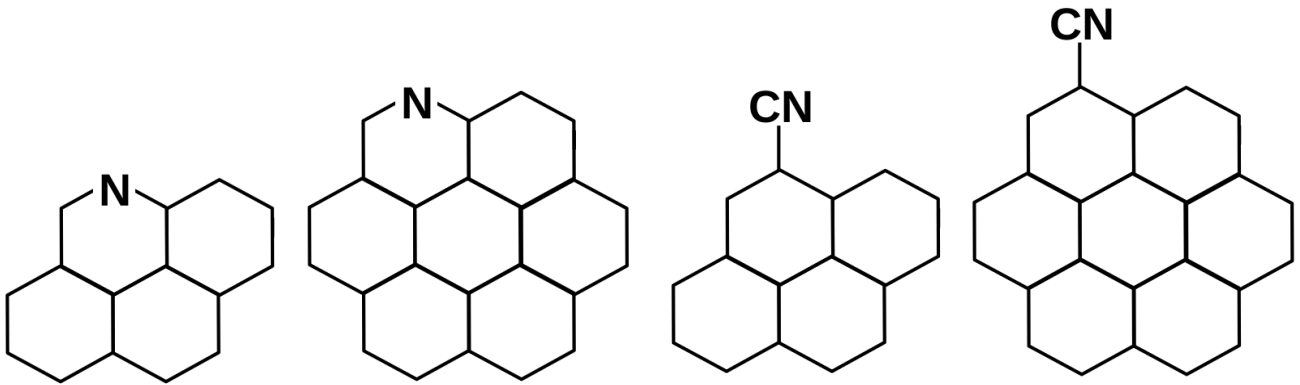
Based on the above, other readily detectable PAH species have been studied, out of which the most prominent and suitable PAH candidates are nitrogen containing PAHs or polycyclic aromatic nitrogen heterocycles (PANHs) (Hudgins et al. 2005). PANHs are

[★] akant.vats@bhu.ac.in

[†] amitpah@gmail.com



(a) Benzonitrile, 1-cyano-naphthalene and quinoline (from left to right).



(b) N-pyrene, N-coronene, CN-pyrene and CN-coronene (from left to right).

Figure 1. N-containing species considered here as (a) test molecules and (b) target molecules.

strongly polar in nature, likely widespread in the ISM and possible carriers of the UIR band at $6.2\ \mu\text{m}$ (Hudgins et al. 2005; Ricca et al. 2021; Vats et al. 2022). PANHs have been detected in carbonaceous meteorites (Sephton 2002) and in the form of PAH nitriles, such as benzonitrile ($\text{C}_6\text{H}_5\text{CN}$), 1-cyano-1, 3-cyclopentadiene ($\text{C}_5\text{H}_6\text{CN}$), and 1- and 2-cyano-naphthalene ($\text{C}_{11}\text{H}_7\text{CN}$) in the TMC-1, a cold, dark molecular cloud (McGuire et al. 2018; McCarthy et al. 2021; McGuire et al. 2021). This confirms a significant presence of PANHs in the ISM.

Recent technological developments in single dish and interferometry radio antennas have resulted in facilities with great sensitivity and resolution (such as the Atacama Large Millimeter Array (ALMA)), driving up demand for more precise rotational spectroscopic data. However, experimental studies regarding pure rotational spectra of PANHs are limited in number and restricted to small PAH species (within 12 C atoms). Therefore, theoretical methodologies might be more convenient to study PANHs. The complete interpretation of AME requires pure rotational spectroscopic data on PAHs/PANHs and other dust-correlated carbonaceous species.

In the present work, the pure rotational spectra of PANHs are computed and analyzed theoretically in the frequency range of 8 to 33 GHz, relevant to the interstellar search of aromatic molecules (Ali-Haïmoud et al. 2015; McGuire et al. 2018, 2021; McCarthy

et al. 2021). The accuracy of the computational methods adopted in this work has been verified before applying on the target PANH molecules. The main aim of this work is to provide the pure rotational data of large PANH molecules to explore their possibility of detection in the ISM. The paper is organized as follows. Section 2 describes the selection of the sample and theoretical methods. Section 3.1 presents the effect of different basis sets on rotational constants and establishes the accuracy of the calculation methods used. The results are discussed in Section 3.2. Section 4 discusses the astrophysical implications with conclusions.

2 SAMPLE AND THEORETICAL METHODS

The comparison of the UIR bands with theoretical IR spectra suggests the abundance of symmetric and compact PAHs in the ISM (Bauschlicher et al. 2009; Ricca et al. 2012). The substitution of N atom in compact PAH forms a quasi-symmetric and strongly polar PANH molecule having well-identifiable rotational spectra (Ali-Haïmoud et al. 2015). Thus, PANHs are suitable candidates to be studied for PAH rotational spectroscopy. There are two most appropriate forms of PANHs— (i) PAHs having N within the PAH skeleton or N-substituted PAHs (N-PAHs, Fig. 1) (Hudgins et al. 2005; Ricca et al. 2021; Vats et al. 2022) and, (ii) PAH nitriles or CN-attached PAHs (CN-PAHs, Fig. 1). Based on this, we consider

Table 1. Rotational spectral parameters of benzonitrile (C_6H_5CN), 1-cyanonaphthalene ($C_{10}H_7CN$) and quinoline (C_9H_7N). The deviation[†] between the experimental and theoretical values are given in parentheses.

Constants	Experimental	B3LYP 6-311+G(d,p)	B3LYP cc-pVTZ	MP2 6-31G(d,p)
$C_6H_5CN^\dagger$				
A_0^a (MHz)	5655.2652	5673.8318 (0.32)	5703.7911 (0.85)	5657.1971 (0.03)
B_0 (MHz)	1546.8758	1548.3016 (0.09)	1555.2297 (0.53)	1535.6142 (0.73)
C_0 (MHz)	1214.4040	1216.3723 (0.16)	1222.0247 (0.62)	1207.7712 (0.54)
Δ_J^b (Hz)	45.6	43.2	43.4	41.9
Δ_{JK} (Hz)	933.1	865.6	898.2	924.6
Δ_K (Hz)	272	285	263	196
δ_J (Hz)	11.10	10.43	10.53	10.20
δ_K (Hz)	613	561	578	590
χ_{xx}^c (MHz)	-4.237	-4.04	-4.41	-3.98
χ_{yy} (MHz)	2.289	2.19	2.38	2.17
χ_{zz} (MHz)	1.949	1.85	2.03	1.81
μ^d (Debye)	$\mu_a = 4.5152$	$\mu_a = 4.7426$	$\mu_a = 4.6447$	$\mu_a = 5.0092$
$C_{10}H_7CN^\ddagger$				
A_0^a (MHz)	1478.8483	1488.1689 (0.62)	1493.7911 (1.01)	1473.1330 (0.38)
B_0 (MHz)	956.7842	950.3583 (0.67)	960.0357 (0.33)	954.1701 (0.27)
C_0 (MHz)	580.9889	579.9785 (0.10)	584.4317 (0.58)	579.0868 (0.32)
Δ_J^b (Hz)	39.636	37.005	37.199	40.224
Δ_{JK} (Hz)	-159.63	-140.66	-137.32	-151.57
Δ_K (Hz)	249.40	223.72	221.93	232.48
δ_J (Hz)	17.94	16.19	16.98	17.72
δ_K (Hz)	10.29	10.81	10.93	11.72
χ_{xx}^c (MHz)	1.92	1.97	2.12	1.99
χ_{yy} (MHz)	2.98	2.50	2.60	2.71
χ_{zz} (MHz)	-4.90	-4.47	-4.73	-4.52
μ^d (Debye)		$\mu_a = 3.6616$ $\mu_b = 3.0372$	$\mu_a = 3.5632$ $\mu_b = 2.9645$	$\mu_a = 3.7782$ $\mu_b = 3.2877$
$C_9H_7N^*$				
A_0^a (MHz)	3145.5330	3154.9974 (0.29)	3171.7536 (0.82)	3139.9102 (0.17)
B_0 (MHz)	1271.5779	1271.2549 (0.02)	1277.5652 (0.46)	1271.2024 (0.02)
C_0 (MHz)	905.7394	906.1403 (0.04)	910.7285 (0.54)	904.8712 (0.09)
Δ_J^b (Hz)	19.110	18.389	18.533	18.687
Δ_{JK} (Hz)	47.031	46.456	46.883	46.891
Δ_K (Hz)	161.461	161.222	162.859	163.024
δ_J (Hz)	5.662	5.448	5.492	5.501
δ_K (Hz)	60.622	58.611	59.160	60.148
χ_{xx}^c (MHz)	-4.684	-4.682	-4.925	-4.302
χ_{yy} (MHz)	3.221	3.219	2.866	2.791
χ_{zz} (MHz)	1.462	1.458	1.455	1.502
μ^d (Debye)	$\mu_a = 0.1435$ $\mu_b = 2.0146$	$\mu_a = 0.2367$ $\mu_b = 2.1572$	$\mu_a = 0.2014$ $\mu_b = 2.0314$	$\mu_a = 0.216$ $\mu_b = 2.012$

Notes. [†]Relative error = $\frac{\text{exp.}-\text{theo.}}{\text{theo.}} \times 100$.

^aRotational constants, ^bQuartic centrifugal distortion constants, ^c ^{14}N quadrupole coupling constants in reference to the principal axis system, ^dDipole moment.

[†]McGuire et al. (2018), [‡]McNaughton et al. (2018), ^{*}Kisiel et al. (2003).

nitrogen substitution in two symmetric and compact PAHs [pyrene ($C_{16}H_{10}$) and coronene ($C_{24}H_{12}$)] having substantial photostability against UV radiation. For N-PAHs, there are two possibilities for N-inclusion in PAHs; exoskeletal (exo-PANHs), where the N atom replaces CH at the periphery, and endoskeletal (endo-PANHs), where N is incorporated within the PAH structure in place of C. There is very little impact on the molecular stability when N is substituted in the exoskeletal manner, however, the incorporation of N atom within the ring causes an excess charge and higher electron repulsion, which reduces stability (Ricca et al. 2021). Therefore,

the present study considers the N-PAHs, where N is substituted at the periphery.

Since there are no laboratory rotational studies available for pyrene and coronene in N- and CN-PAH variants, we have selected 3 N-containing molecules for establishing the accuracy of our computational method. These molecules are benzonitrile (C_6H_5CN), 1-cyanonaphthalene ($C_{10}H_7CN$), (CN-PAHs) and quinoline (C_9H_7N), where N replaces CH at the periphery (N-PAH). The first two have recently been discovered in the ISM (McGuire et al. 2018, 2021), whereas the third has been proposed for identification and

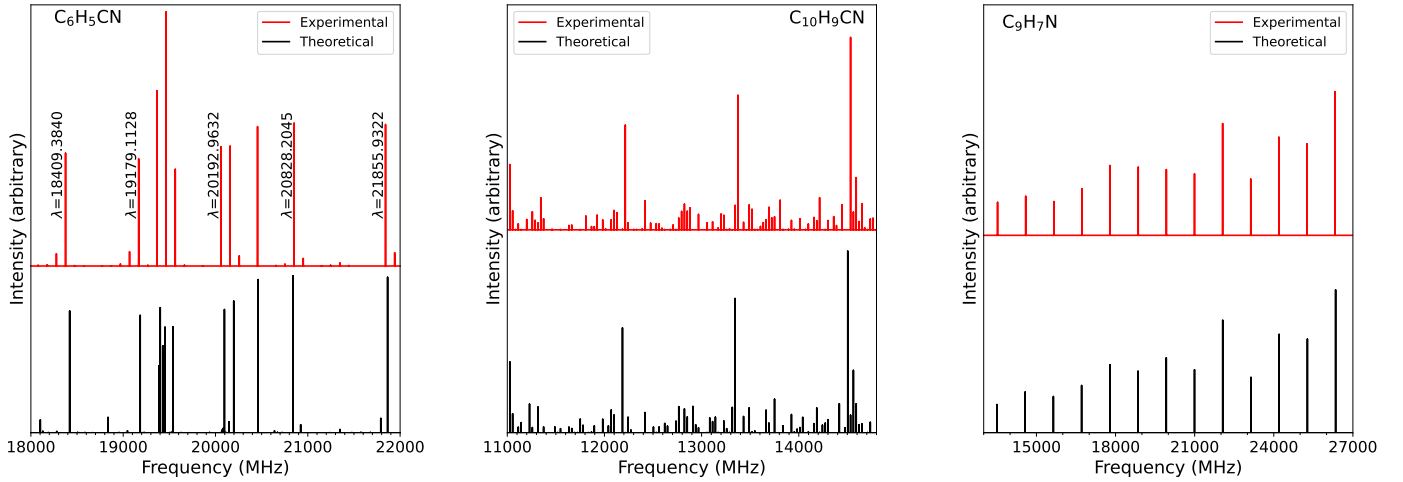


Figure 2. Rotational spectra of benzonitrile (C_6H_5CN), 1-cyanonaphthalene ($C_{10}H_7CN$) and quinoline (C_9H_7N) with B3LYP/6-311+G(d,p) at 300 K (black) in the centimetre-wave region. The experimental spectra are shown in red. The band positions of detected emission lines of benzonitrile in the TMC-1 are labelled.

has been explored in a number of studies (Kisiel et al. 2003; Pirali et al. 2015, & references therein).

The GAUSSIAN 09 (Frisch et al. 2009) suite of programs was used to compute each molecule’s geometry, rotational constants, quadrupole coupling constants, quartic centrifugal distortion constants and dipole moments using Density Functional Theory (DFT) with anharmonic vibrational frequency calculations. DFT has been widely utilized in rotational spectroscopy of interstellar N-containing PAHs to determine the molecular or spectroscopic constants (Kisiel et al. 2003; McNaughton et al. 2008; Pirali et al. 2015; McNaughton et al. 2018), as well as to compute their vibrational modes (Hudgins et al. 2005; Vats et al. 2022; Ricca et al. 2021). The use of B3LYP functional with the 6–311+G(d,p) basis set or the correlation-consistent polarized triple valence basis set (cc-pVTZ) are found effective for studying the molecular or spectroscopic constants of CN-PAHs (McNaughton et al. 2018), whereas the MP2/6-31G(d,p) combination is found better for quinoline (Kisiel et al. 2003). As a result, the current study employs all three of the above-mentioned basis sets on the test molecules (Fig. 1-a). The basis set with the best match is then used to compute the target molecules (Fig. 1-b) as well as to simulate the pure rotational spectra.

The pure rotational spectra are simulated using PGOPHER general purpose program (Western 2017). At the second-order vibrational perturbation theory (VPT2) level, rotational-vibrational coupling, anharmonic and quartic centrifugal-distortion corrections were considered to obtain all the simulated spectra. PGOPHER is frequently used in astrophysical context on PANH molecules (Nesvadba et al. 2020; Chitarra et al. 2021). In PGOPHER, the Watson’s A-reduced effective rotational Hamiltonian up to the sixth order terms were coupled with the nuclear quadrupole terms to obtain the transition frequencies and assigned rotational and hyperfine quantum numbers J_{K_a, K_c} and F. Because of the existence of ^{14}N ($I = 1$) nuclei, the lines in the cm region show resolved hyperfine splitting (McNaughton et al. 2018). Therefore, the ^{14}N -nuclear quadrupole hyperfine structure is also simulated for the target molecules in the cm-wave region.

3 RESULTS AND DISCUSSION

3.1 Accuracy of the computational methods

3.1.1 Effects of different basis sets on rotational spectral parameters

Beyond the rigid-rotor approximation, we briefly discuss the most frequent model Hamiltonians for determining the rotational spectroscopic constants of the chosen asymmetric top PANHs. The constants are first derived for the test molecules, benzonitrile, 1-cyanonaphthalene (1-CNN) and quinoline using three distinct basis sets– B3LYP/6-311+G(d,p), B3LYP/cc-pVTZ and MP2/6-31G(d,p). Examining the rotational spectra of PANHs frequently involves the use of these basis sets (Kisiel et al. 2003; McNaughton et al. 2018). The molecular constants calculated at the considered basis sets are given in Table 1 with the deviation between the experimental and theoretical rotational constants’ values shown in parentheses.

For all the test molecules, the ground state rotational constants (A_0 , B_0 and C_0) computed at the B3LYP/6-311+G(d,p) level of theory agree within ~ 0.6 per cent of those determined through experiments. These values are within ~ 0.8 and ~ 0.7 per cent of those obtained from the B3LYP/cc-pVTZ and MP2/6-31G(d,p) level of theory, respectively. The error values are the maximum percentage errors calculated on the rotational constants (Table 1). The mean percentage errors for rotational constants of the test molecules are 0.24, 0.63 and 0.28 with B3LYP/6-311+G(d,p), B3LYP/cc-pVTZ and MP2/6-31G(d,p), respectively. As a result, the ground state rotational constants of N- and CN-PAHs are better estimated by the B3LYP/6-311+G(d,p) level (Table 1).

All the level of computations used here show nearly equal performance in computing the centrifugal distortion constants (Δ_J , Δ_{JK} , Δ_K , δ_J and δ_K). For CN containing PAHs, the computed values match within the mean percentage error of ~ 6.7 per cent compared to the experiments by all the level of theories except Δ_{JK} for 1-CNN. It shows relative error of ~ 13.4 per cent (Table 1) with the B3LYP/6-311+G(d,p). The centrifugal distortion constants of N-PAH-quinoline are predicted to be within ~ 3.4 per cent of the ex-

Table 2. Rotational transitions of ground state of benzonitrile (C_6H_5CN), 1-cyanonaphthalene ($C_{10}H_7CN$) and quinoline (C_9H_7N) with relative error ($\sim \delta$).

Transition $J'_{K'_a, K'_c} \rightarrow J''_{K''_a, K''_c}$	$F' \rightarrow F''$	Frequency		δ (%)
		Experimental [†] (MHz)	Calculated [‡] (MHz)	
C_6H_5CN				
$7_{0,7} \rightarrow 6_{0,6}$	$6 \rightarrow 5$	18409.3490	18438.2834	0.15
$7_{2,6} \rightarrow 6_{2,5}$	$7 \rightarrow 6$	19178.9991	19203.9883	0.13
$7_{2,5} \rightarrow 6_{2,4}$	$8 \rightarrow 7$	20096.0931	20115.8509	0.09
$7_{1,6} \rightarrow 6_{1,5}$	$8 \rightarrow 7$	20192.9641	20217.2728	0.12
$8_{0,8} \rightarrow 8_{0,7}$	$8 \rightarrow 7$	20828.2065	20861.7296	0.16
$8_{2,7} \rightarrow 7_{2,6}$	$8 \rightarrow 7$	21855.9330	21884.8986	0.13
$8_{1,7} \rightarrow 7_{1,6}$	$8 \rightarrow 7$	22943.4750	22972.4289	0.12
$9_{0,9} \rightarrow 8_{0,8}$	$8 \rightarrow 7$	23227.6869	23265.5033	0.16
$C_{10}H_7CN$				
$9_{0,9} \rightarrow 8_{0,8}$	$9 \rightarrow 8$	11039.2815	11020.1694	0.17
$9_{2,8} \rightarrow 8_{2,7}$	$9 \rightarrow 8$	12202.9932	12181.7064	0.17
$9_{2,7} \rightarrow 8_{2,6}$	$10 \rightarrow 9$	13481.0643	13471.1245	0.07
$10_{3,8} \rightarrow 9_{3,7}$	$10 \rightarrow 9$	14525.9246	14498.4194	0.18
C_9H_7N				
$4_{2,3} \rightarrow 3_{1,2}$	$4 \rightarrow 3$	13777.0811	13807.7524	0.22
$14_{3,11} \rightarrow 14_{2,12}$	$14 \rightarrow 14$	14510.9656	14469.6863	0.28
$18_{4,14} \rightarrow 18_{3,15}$	$19 \rightarrow 19$	17853.9280	17786.8871	0.37
$28_{7,21} \rightarrow 28_{6,22}$	$22 \rightarrow 22$	22156.2876	22030.2369	0.57
$18_{7,12} \rightarrow 18_{6,13}$	$18 \rightarrow 18$	25309.5059	25433.3977	0.48
$13_{2,12} \rightarrow 12_{1,11}$	$12 \rightarrow 11$	26422.1001	26439.6661	0.06

[†]The experimental data are taken from McGuire et al. (2018) for C_6H_5CN ; McNaughton et al. (2018) for $C_{10}H_7CN$ and Kisiel et al. (2003) for C_9H_7N .

[‡]B3LYP/6-311+G(d,p).

perimental values by all the level of theories considered here (Table 1).

All the level of theories calculate the nuclear quadrupole coupling constants (χ_{xx} , χ_{yy} and χ_{zz}) to within ~ 10 per cent of the experimental values, where the B3LYP/6-311+G(d,p) level achieves the best performance.

3.1.2 Simulation of rotational spectra with hyperfine splitting

The pure rotational spectra of benzonitrile, 1-CNN and quinoline are shown in Figure 2. These are simulated at 300 K with the B3LYP/6-311+G(d,p) level of theory, in comparison with the experimental spectra in the cm-wave region. Some of the rotational transitions of the test molecules are tabulated in Table 2 with relative error in the experimental and calculated values at the B3LYP/6-311+G(d,p) level. Besides this, the ^{14}N -nuclear quadrupole hyperfine structure for an observed benzonitrile transition, $7_{0,7} \rightarrow 6_{0,6}$ ($J'_{K'_a, K'_c} \rightarrow J''_{K''_a, K''_c}$ with $F = J + I$) in the TMC-1 is also shown in Figure 3.

In comparison with the experimental values, the transition frequencies are computed to within ~ 0.18 per cent for the CN-PAH and within ~ 0.5 per cent for the N-PAH considered here (Table 2 & Figure 2). Even small variations in the rotational constants' precision in spectral simulations have a big impact on how well the line frequencies are predicted. The perusal of Table 2 reveals that the discrepancies between the experimental and theoretical transitions are larger for the N-PAH (C_9H_7N) despite having more accurate prediction of rotational constants (A_0 , B_0 , C_0) compared to the CN-PAHs (Table 1). This indicates a significant dominance of the A_0 rotational constant in the simulation of the N-PAH rotational

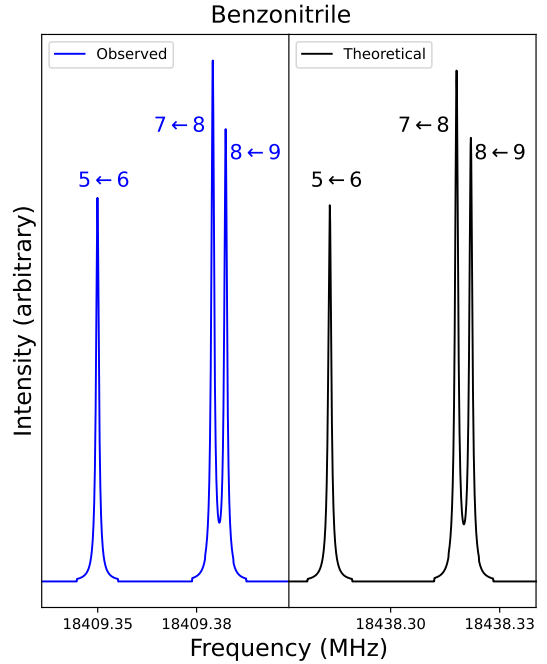


Figure 3. ^{14}N -nuclear quadrupole hyperfine components of the $7_{0,7} \rightarrow 6_{0,6}$ transition with $F'' \rightarrow F'$ shown in blue and black colors for the observed and simulated benzonitrile transition, respectively, with the B3LYP/6-311+G(d,p) level.

spectrum, which, in the case of CN-PAHs, appears to be the least dominating.

The ^{14}N -nuclear quadrupole hyperfine structure simulation of $7_{0,7} \rightarrow 6_{0,6}$ benzonitrile observed transition shown in Figure 3 is well resolved, which proves the usefulness of the applied method in simulating the hyperfine structure of the PANH molecules that have been taken into consideration.

Based on the above, it is evident that the B3LYP/6-311+G(d,p) level of theory is an appropriate level for estimating molecular constants and simulating rotational spectrum with hyperfine structure for both N-PAH and CN-PAH variants. As a result, in the following section, two comparatively large PAHs, pyrene ($C_{16}H_{10}$) and coronene ($C_{24}H_{12}$) for both the N and CN substituted variants are investigated with the B3LYP/6-311+G(d,p) level of theory.

3.2 Pure rotational spectroscopy of target PAHs

N-PAHs are believed to represent a substantial portion of the astronomical PAH population and CN-PAHs have already been detected in the ISM. They both exhibit strong polarity and stand out as the most potential target for pure rotational spectroscopy. In this light, based on the finding examined in the previous section, the molecular constants and rotational spectra of pyrene ($C_{16}H_{10}$) and coronene ($C_{24}H_{12}$) in both the N-PAH and CN-PAH variants are given with the B3LYP/6-311+G(d,p) level of theory. It is apparent that the dipole moment components for each of these planar molecules are restricted to the plane of the PAH, i.e., $\mu_c = 0$ (Table 3).

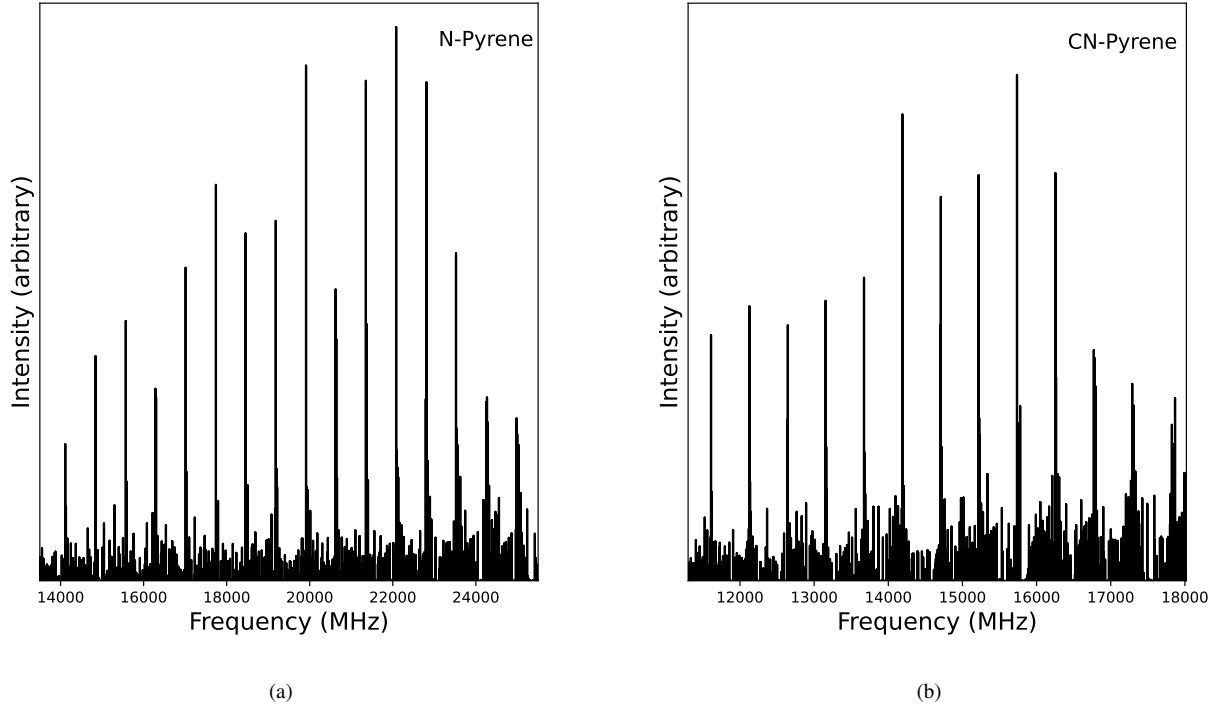


Figure 4. Rotational spectrum simulation of pyrene in N-PAH and CN-PAH variants at 300 K with B3LYP/6-311+G(d,p) level.

Table 3. Rotational spectral parameters of pyrene and coronene in N-PAH and CN-PAH variant with B3LYP/6-311+G(d,p) level.

Constants	Pyrene		Coronene	
	N-PAH	CN-PAH	N-PAH	CN-PAH
A_0^a (MHz)	1018.8042	846.1307	337.4456	333.9216
B_0 (MHz)	561.3018	371.0981	333.6118	221.1045
C_0 (MHz)	361.9103	257.9608	167.7588	133.0236
Δ_J^b (Hz)	2.25	1.91	0.89	0.20
Δ_{JK} (Hz)	1.09	-4.9	-1.44	0.24
Δ_K (Hz)	11.51	19	0.62	0.81
δ_J (Hz)	0.78	0.69	0.008	0.071
δ_K (Hz)	4.07	3.11	0.53	0.61
χ_{xx}^c (MHz)	-4.412	2.365	-4.844	2.407
χ_{yy} (MHz)	3.362	2.034	3.383	1.935
χ_{zz} (MHz)	1.428	-4.399	1.461	-4.342
μ^d (Debye)	$\mu_a = 1.8904$ $\mu_b = 2.1205$ $\mu_{tot.} = 2.8408$	$\mu_a = 3.6716$ $\mu_b = 4.0694$ $\mu_{tot.} = 5.4809$	$\mu_a = 2.2535$ $\mu_b = 1.5565$ $\mu_{tot.} = 2.7388$	$\mu_a = 1.1782$ $\mu_b = 5.4072$ $\mu_{tot.} = 5.5341$

Notes. ^aRotational constants, ^bQuartic centrifugal distortion constants, ^c ^{14}N quadrupole coupling constants in reference to the principal axis system, ^dDipole moment.

3.2.1 Pyrene

The molecular constants of pyrene in N-PAH and CN-PAH variants are given in Table 3 and the simulation of a portion of the cm-wave spectra is shown in Figure 4. In pyrene, the ground state rotational constants (A_0 , B_0 , C_0) are large for N-variant compared to the CN-

variant. For example, the A_0 rotational constant is 1018.8042 MHz for N-pyrene while for CN-pyrene, the value is 846.1307 MHz (Table 3). The average difference between the rotational constants of N- and CN-pyrene is ~ 150 MHz, where the maximum difference is observed for the B_0 . With the exception of the Δ_K , the centrifugal distortion constants are also large for N-pyrene. The ^{14}N

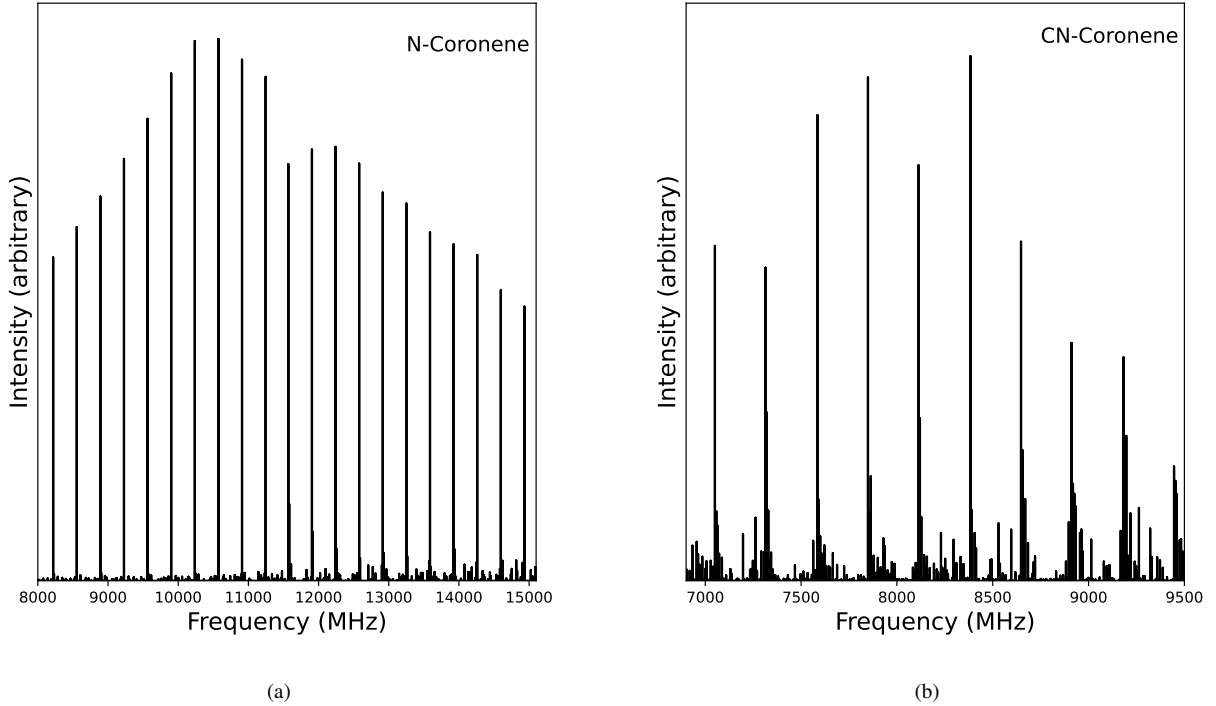


Figure 5. Same as Fig. 4 for Coronene.

quadrupole coupling constants of N-pyrene and CN-pyrene show similar values to their counterpart species given in Table 1 (quinoline and 1-CNN, respectively). For example, the χ_{zz} is 1.428 MHz for N-pyrene and 1.462 MHz for quinoline, for CN-pyrene, the χ_{zz} differs with 1-CNN by only 0.07 MHz. These small changes in $\chi(N)$ clearly indicates that the N atom’s local electronic structure is independent from the proximity of the atomic ring. CN-PAHs seem to be strongly polar compared to similar-sized N-PAHs. The magnitude of the dipole moments are larger for CN-pyrene, which is consistent with the trend shown in Table 1 for the N-PAH (quinoline) and CN-PAH (1-CNN).

The region with the strongest transitions at 300 K in the cm-wave spectra of N-pyrene and CN-pyrene are shown in Figure 4(a) and Figure 4(b), respectively. The strongest lines fall in the K (18–27 GHz) band for N-pyrene, whereas for CN-pyrene, the strongest transitions are found in the K_u (12–18 GHz) band. At 300 K, the strongest line appears around 22 GHz for N-pyrene (Figure 4-a) and near 16 GHz for CN-pyrene (Figure 4-b).

3.2.2 Coronene

Table 3 presents the molecular constants of N-coronene and CN-coronene while their rotational spectra in the cm-wave region are presented in Figure 5. The rotational constants are large for N-PAH variant for coronene as well, however, the average difference in the rotational constants between N- and CN-coronene is ~ 50 MHz, which is lower than the difference seen for pyrene (Table 3). Similar to pyrene, the rotational constant B_0 in coronene exhibits the max-

imum difference between its N- and CN-PAH variant. In coronene, the centrifugal distortion constants are higher for the CN-PAH variant except the Δ_J . The ^{14}N quadrupole coupling constants of N-coronene and CN-coronene show similar behavior to pyrene (Table 3). The CN-PAH version is more polar compared to the N-PAH for coronene as well.

The cm-wave spectra of coronene with strongest lines at 300 K are displayed in Figure 5(a) for N-PAH while in Figure 5(b) for CN-PAH. For both the N- and CN-coronene, the strongest transitions lie within X (8–12 GHz) band. The strongest lines at 300 K are found near 11 GHz and 8.5 GHz for N-coronene (Figure 5-a) and CN-coronene (Figure 5-b), respectively.

4 ASTROPHYSICAL IMPLICATIONS AND CONCLUSIONS

In radio astronomy, the strength of a molecule’s permanent dipole moment is a major factor in its ability to be detected in the ISM. Interstellar molecules are mostly discovered in space at radio frequencies using pure rotational spectroscopy. The CN-PAHs are found to be far more polar compared to the N-PAHs, with average dipole moment values of 5.5 and 2.7 D for the CN-PAHs and N-PAHs, respectively. The search of N- and CN-PAHs with radio telescopes has been undertaken towards cold molecular clouds, such as Taurus molecular cloud (TMC-1) (McGuire et al. 2018, 2021) and Perseus molecular cloud (Ali-Haïmoud et al. 2015). In these clouds, the rotational transitions of PAH-related species are thought to be the strongest in the 8–33.5 GHz frequency range with

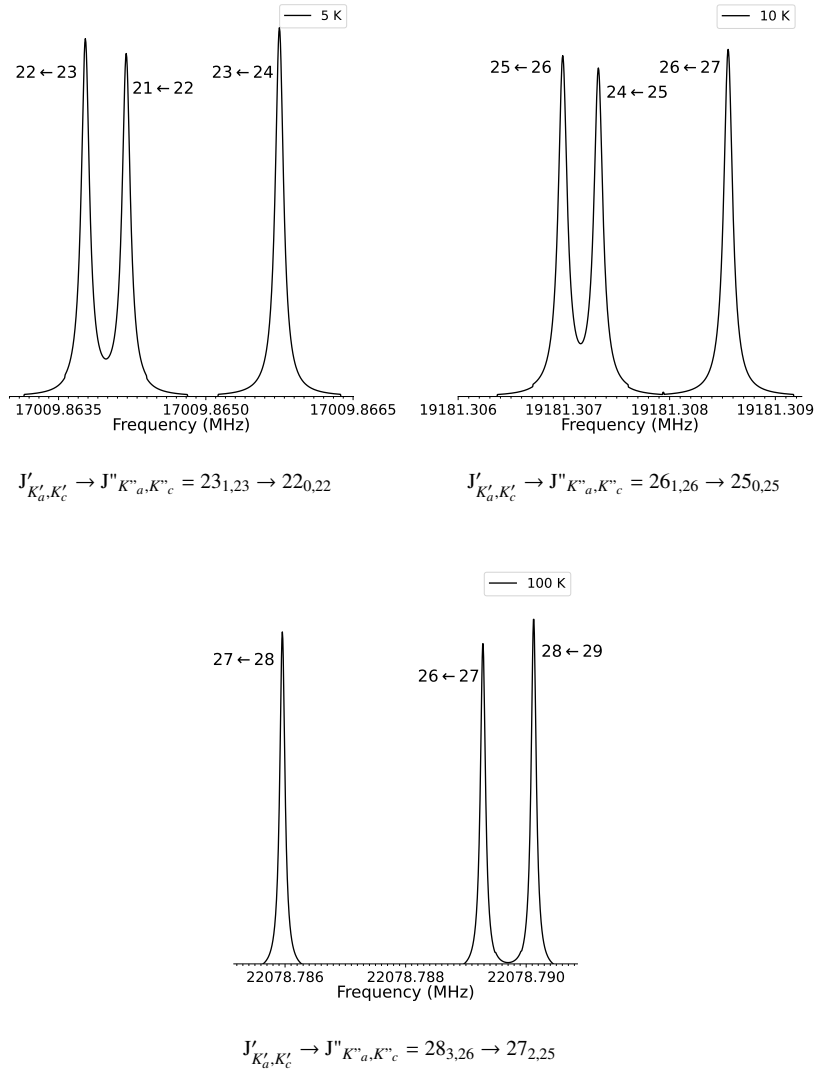


Figure 6. The strongest transition of N-pyrene showing resolved hyperfine structure at 5, 10 and 100 K temperatures without accounting for Doppler splitting.

typical temperature range of 5–10 K (McGuire et al. 2020). The only PAH species discovered so far in the ISM are CN-PAHs; 1- and 2-cyanonaphthalene (McGuire et al. 2021).

We report the cm-wave spectra of N- and CN-pyrene ($C_{16}H_{10}$) and N- and CN-coronene ($C_{24}H_{12}$) for the first time. The B3LYP/6-311+G(d,p) level of theory computes the rotational constants within ~ 0.6 per cent of those obtained experimentally for all the N- and CN-PAHs used here as test molecules. For rotational transition frequencies, the B3LYP/6-311+G(d,p) level achieves best performance here and shows relative errors of ~ 0.5 and ~ 0.18 per cent between experimental and theoretical values for N-PAH and CN-PAHs, respectively. As a result, the same level of theory has also been utilized for computing the molecular constants and rotational spectra of pyrene and coronene in N-PAH and CN-PAH variants. The data presented here may be directly utilized to detect these PAHs in potential ISM environments.

While taking interstellar detection into the consideration, the hyperfine resolved structure might play a significant role for the considered PANH species as the splitting in the cm-wave region

is found to be similar with the linewidths measured for a typical cold, dark molecular clouds— e.g., TMC-1 (Buchanan et al. 2021). Therefore, the ^{14}N quadrupole hyperfine resolved structures are also given for the strongest transitions of the considered N- and CN-PAH molecules at 5, 10 and 100 K.

4.0.1 Pyrene

The hyperfine resolved structures are shown at 5, 10 and 100 K in Figure 6 and Figure 7 for N- and CN-pyrene, respectively while the transition frequencies are tabulated in Table 4. The complete rotational spectra at 10, 100 and 300 K are given in Figure A1. For both N- and CN-pyrene, the strongest lines lie at cm-wavelengths at low as well as some warmer temperatures. As temperature increases, the larger partition function significantly reduces the strength of transitions (Figure A1). For N-pyrene: at 5 K, the strongest transition is $J'=23$ around 17 GHz falling in K_u band whereas at 10 K and 100 K, the strongest transitions lie within K band, correspond-

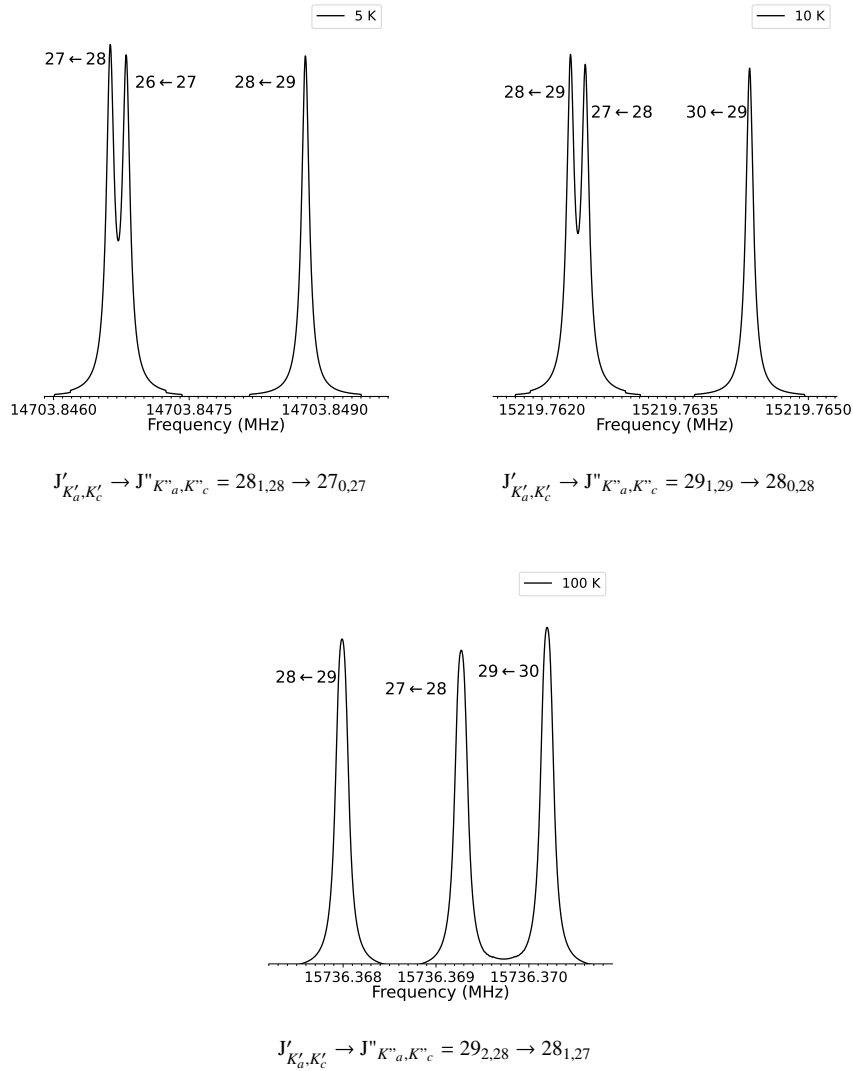


Figure 7. Same as Figure 6 for CN-pyrene.

ing to $J'=26$ and $J'=28$ near 19.1 and 22 GHz, respectively (Fig. 6 and Table 4).

For CN-pyrene: at 5, 10 and 100 K, the strongest lines fall in K band. The strongest transition at 5 K is $J'=28$ near 14 GHz while at 10 and 100 K, the strongest lines correspond to $J'=29$ around 15.2 and 15.7 GHz, respectively (Fig. 7 and Table 4).

4.0.2 Coronene

For coronene, Figure 8 and Figure 9 show hyperfine splitting of the strongest rotational transition of N- and CN-coronene, respectively at 5, 10 and 100 K, which are tabulated in Table 4. The corresponding rotational spectra in the complete wavelength range are shown in Figure A1. The strongest lines in coronene are present at shorter wavelengths compared to pyrene at each temperature (Figure A1). In terms of the intensity, the transitions in coronene are weaker than those in pyrene for both the N- and CN-PAH variants (Figure A1) due to its larger rotational partition function that depends on

rotational constants (A, B and C) ($Q_{\text{rot}} \propto \sqrt{\frac{T^3}{ABC}}$, where T is temperature).

The strongest lines of N-coronene fall in X band (8–12 GHz) at cold and some warmer temperatures (Figure 8). The strongest transitions of N-coronene at 5, 10 and 100 K are $J'=28$, $J'=29$ and $J'=30$ around 9.5, 9.8 and 10.2 GHz, respectively. For CN-coronene, the wavelengths are shorter than those of N-coronene and this behavior is consistent with that of pyrene (Table 4). The strongest transitions of CN-coronene at 5, 10 and 100 K correspond to $J'=28$, $J'=29$ and $J'=28$ near 7.5, 7.8 and 8.1 GHz, respectively.

Based on the large permanent dipole moment, CN-PAHs are the most suitable PAH variant to be searched for in the ISM. Furthermore, the smaller partition function in pyrene renders CN-pyrene an excellent candidate to be found in cold, dark molecular clouds such as the TMC-1. The search for CN-pyrene in molecular clouds like TMC-1 is supported by the following arguments.

It is believed that the PAHs form in carbon-rich circumstellar environments (CSEs), where there is a significant elemental abundance of nitrogen (Reddy et al. 1999). As a result, the PAH fam-

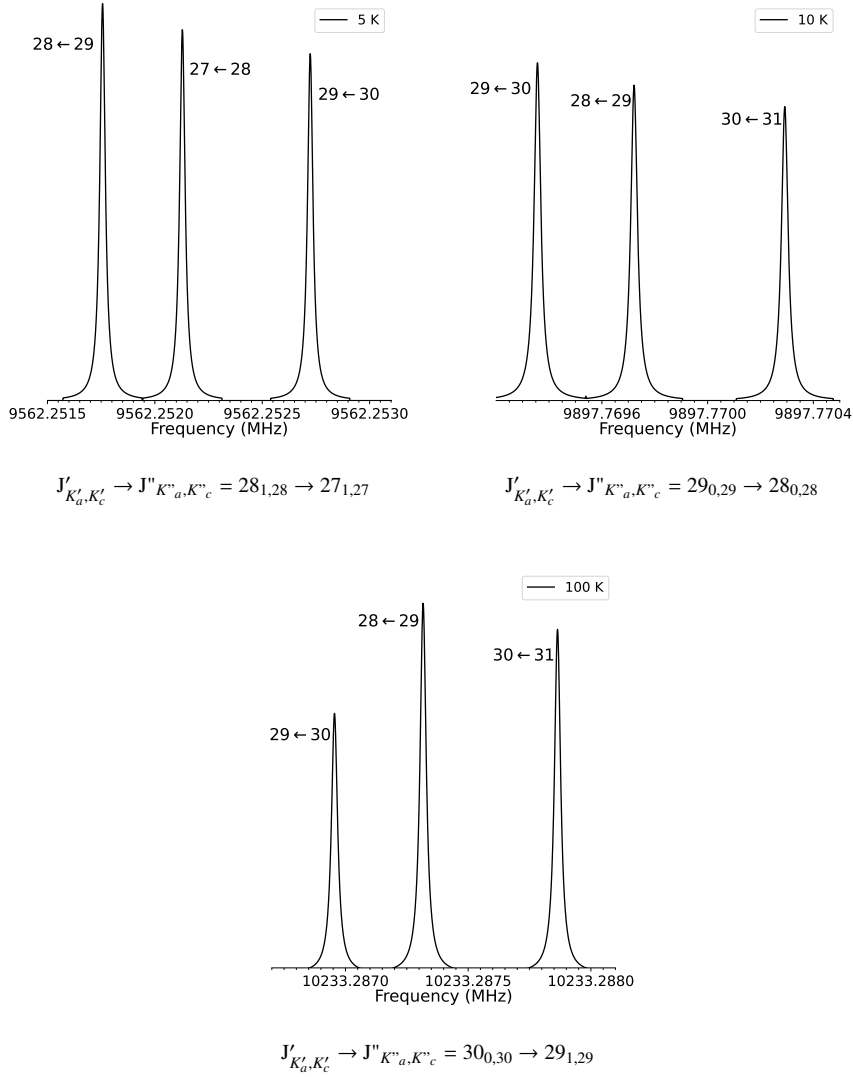


Figure 8. Same as Figure 6 for N-coronene.

ily members that are ejected into the ISM from CSEs and PNe include a mixture of pure PAHs, CN-PAHs, and N-PAHs (Allamandola et al. 2021). Pure PAH lacks the permanent dipole moment and does not show a pure rotational spectrum. For N-containing PAHs, the detection through rotational lines might be hampered in the regions exhibiting the strong $6.2 \mu\text{m}$ band due to the following reasons. Large-sized PANHs show smaller rotational constants thus possess larger partition functions (Hudgins et al. 2005; Tielsens 2008) and PAHs with more than ~ 40 – 50 C atoms are thought to be more relevant to be found in such regions. Their radiated power might be dispersed over many weak lines, which makes their detection quite challenging (Ali-Haïmoud 2014).

The detection of CN-PAHs in TMC-1 is remarkable because it appears that they were formed in the cold, dark molecular cloud itself. It is plausible that alternative interstellar PAH formation mechanisms and chemistry exist in such molecular clouds because the detected PAHs are too small to persist in the diffuse ISM (McGuire et al. 2021; Allamandola et al. 2021). The present work may also be crucial for guiding laboratory experiments and inspiring future

experimental work on the rotational spectroscopy of CN-PAHs and N-PAHs.

ACKNOWLEDGEMENTS

We thank to the anonymous reviewer for the comments and suggestions that helped in bringing clarity to this work. AV acknowledges research fellowship from DST SERB (SERB-EMR/2016/005266) and UGC. AP acknowledges financial support from DST SERB (SERB-CRG/2021/000907), IoE incentive grant, BHU (incentive/2021-22/32439), Banaras Hindu University, Varanasi and thanks the Inter-University Centre for Astronomy and Astrophysics, Pune for associateship. The authors also acknowledge support from DST JSPS grant (DST/INT/JSPS/P-238/2017).

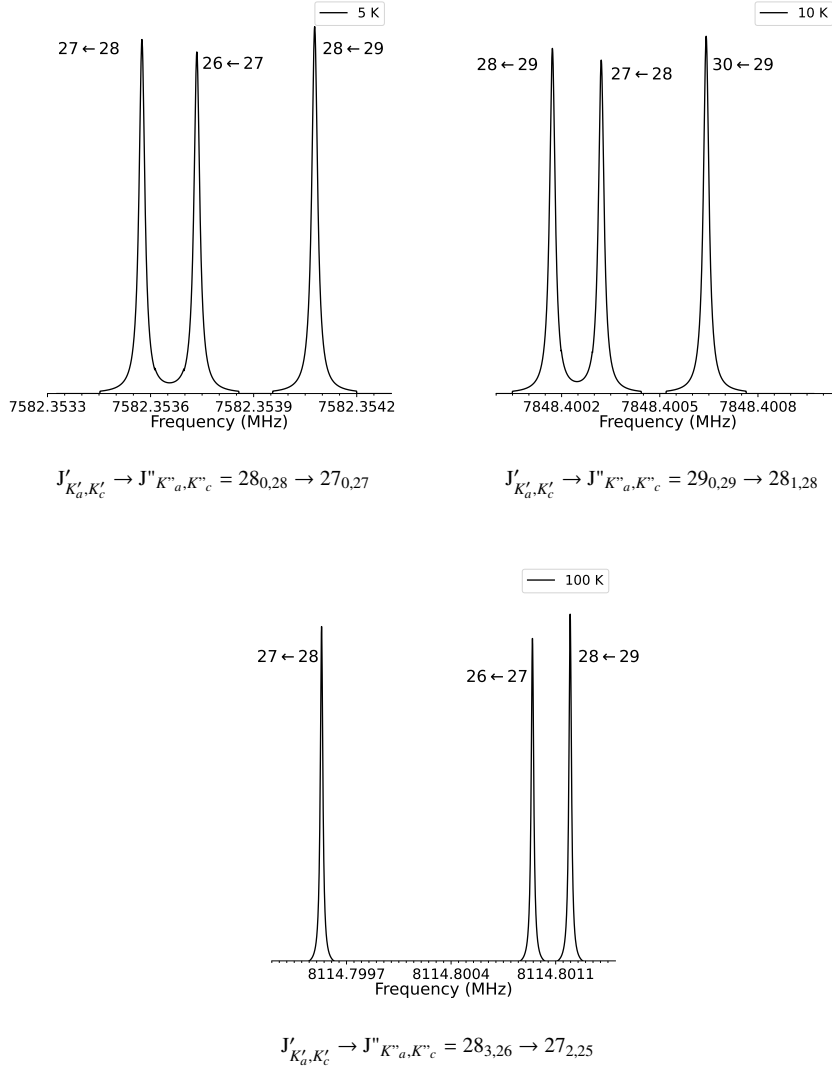


Figure 9. Same as Figure 6 for CN-coronene.

DATA AVAILABILITY

The data used in this article will be shared upon reasonable request to corresponding author.

REFERENCES

- Ali-Haïmoud Y., 2014, *MNRAS*, **437**, 2728
- Ali-Haïmoud Y., Pérez L. M., Maddalena R. J., Roshi D. A., 2015, *MNRAS*, **447**, 315
- Allamandola L. J., Tielens A. G. G. M., Barker J. R., 1985, *ApJ*, **290**, L25
- Allamandola L. J., Tielens A. G. G. M., Barker J. R., 1989, *ApJS*, **71**, 733
- Allamandola L. J., Boersma C., Lee T. J., Bregman J. D., Temi P., 2021, *ApJ*, **917**, L35
- Bauschlicher Charles W. J., Peeters E., Allamandola L. J., 2009, *ApJ*, **697**, 311
- Buchanan Z., Lee K. L. K., Chitarra O., McCarthy M. C., Pirali O., Martin-Drumel M.-A., 2021, *Journal of Molecular Spectroscopy*, **377**, 111425
- Chitarra O., Lee K. L. K., Buchanan Z., Melosso M., McGuire B. A., Goubet M., Pirali O., Martin-Drumel M.-A., 2021, *A&A*, **652**, A163
- Cohen M., Allamandola L., Tielens A. G. G. M., Bregman J., Simpson J. P., Witteborn F. C., Wooden D., Rank D., 1986, *ApJ*, **302**, 737
- Frisch M. J., et al., 2009, Gaussian 09 Revision A.2
- Gillet F. C., Forrest W. J., Merrill K. M., 1973, *ApJ*, **183**, 87
- Hensley B. S., Murray C. E., Dodici M., 2022, *The Astrophysical Journal*, **929**, 23
- Hony S., Van Kerckhoven C., Peeters E., Tielens A. G. G. M., Hudgins D. M., Allamandola L. J., 2001, *A&A*, **370**, 1030
- Hudgins D. M., Bauschlicher Charles W. J., Allamandola L. J., 2005, *ApJ*, **632**, 316
- Kisiel Z., Desyatnyk O., Pszczółkowski L., Charnley S. B., Ehrenfreund P., 2003, *Journal of Molecular Spectroscopy*, **217**, 115
- Kogut A., et al., 1996, *ApJ*, **470**, 653
- Leger A., Puget J. L., 1984, *A&A*, **500**, 279
- Leitch E. M., Readhead A. C. S., Pearson T. J., Myers S. T., 1997, *ApJL*, **486**, L23
- Li A., 2020, *Nature Astronomy*, **4**, 339
- McCarthy M. C., et al., 2021, *Nature Astronomy*, **5**, 176
- McGuire B. A., Burkhardt A. M., Kalenskii S., Shingledecker C. N., Remijan A. J., Herbst E., McCarthy M. C., 2018, *Science*, **359**, 202
- McGuire B. A., et al., 2020, *ApJ*, **900**, L10

Table 4. Hyperfine resolved strongest rotational transitions of pyrene and coronene in N- and CN-PAH variants.

Transition		Frequency	T
$J'_{K'_a, K'_c} \rightarrow J''_{K''_a, K''_c}$	$F' \rightarrow F''$	(MHz)	(K)
N-pyrene			
$23_{1,23} \rightarrow 22_{0,22}$	23 \rightarrow 22	17009.8637	5
	22 \rightarrow 21	17009.8641	
	24 \rightarrow 23	17009.8657	
$26_{1,26} \rightarrow 25_{0,25}$	26 \rightarrow 25	19181.3069	10
	25 \rightarrow 24	19181.3073	
	27 \rightarrow 26	19181.3085	
	28 \rightarrow 27	22078.7859	
$28_{3,26} \rightarrow 27_{2,25}$	27 \rightarrow 26	22078.7892	100
	29 \rightarrow 28	22078.7901	
CN-pyrene			
$28_{1,28} \rightarrow 27_{0,27}$	28 \rightarrow 27	14703.8466	5
	27 \rightarrow 26	14703.8468	
	29 \rightarrow 28	14703.8487	
$29_{1,29} \rightarrow 28_{0,28}$	29 \rightarrow 28	15219.7623	10
	28 \rightarrow 27	15219.7624	
	30 \rightarrow 29	15219.7643	
	29 \rightarrow 28	15736.3680	
$29_{2,28} \rightarrow 28_{1,27}$	28 \rightarrow 27	15736.3693	100
	30 \rightarrow 29	15736.3702	
N-coronene			
$28_{1,28} \rightarrow 27_{1,27}$	29 \rightarrow 28	9562.2517	5
	28 \rightarrow 27	9562.2522	
	30 \rightarrow 29	9562.2527	
$29_{0,29} \rightarrow 28_{0,28}$	30 \rightarrow 29	9897.7693	10
	29 \rightarrow 28	9897.7697	
	31 \rightarrow 30	9897.7702	
	30 \rightarrow 29	10233.2869	
$30_{1,30} \rightarrow 29_{1,29}$	29 \rightarrow 28	10233.2873	100
	31 \rightarrow 30	10233.2878	
CN-coronene			
$28_{0,28} \rightarrow 27_{1,27}$	28 \rightarrow 27	7582.3535	5
	27 \rightarrow 26	7582.3537	
	29 \rightarrow 28	7582.3549	
$29_{0,29} \rightarrow 28_{1,28}$	29 \rightarrow 28	7848.4001	10
	28 \rightarrow 27	7848.4003	
	30 \rightarrow 29	7848.4006	
	28 \rightarrow 27	8114.7995	
$28_{3,26} \rightarrow 27_{2,25}$	27 \rightarrow 26	8114.8010	100
	29 \rightarrow 28	8114.8011	

McGuire B. A., et al., 2021, *Science*, 371, 1265
McNaughton D., Godfrey P. D., Brown R. D., Thorwirth S., Grabow J.-U., 2008, *ApJ*, 678, 309
McNaughton D., Jahn M. K., Travers M. J., Wachsmuth D., Godfrey P. D., Grabow J.-U., 2018, *MNRAS*, 476, 5268
Nesvadba R., Vávra K., Luková K., Kania P., Koucký J., Urban Š., 2020, *J. Quant. Spectrosc. Radiative Transfer*, 249, 107033
Onaka T., 2004, in Witt A. N., Clayton G. C., Draine B. T., eds, *Astronomical Society of the Pacific Conference Series Vol. 309, Astrophysics of Dust*, p. 163
Onaka T., Yamamura I., Tanabe T., Roellig T. L., Yuen L., 1996, *PASJ*, 48, L59
Peeters E., Hony S., Van Kerckhoven C., Tielens A. G. G. M., Allamandola L. J., Hudgins D. M., Bauschlicher C. W., 2002, *A&A*, 390, 1089
Pilleri P., et al., 2009, *MNRAS*, 397, 1053
Pirali O., Kisiel Z., Goubet M., Gruet S., Martin-Drumel M. A., Cuisset A.,

Hindle F., Mouret G., 2015, *J. Chem. Phys.*, 142, 104310
Reddy B. E., Bakker E. J., Hrivnak B. J., 1999, *ApJ*, 524, 831
Ricca A., Bauschlicher Charles W. J., Boersma C., Tielens A. G. G. M., Allamandola L. J., 2012, *ApJ*, 754, 75
Ricca A., Boersma C., Peeters E., 2021, *ApJ*, 923, 202
Salama F., Galazutdinov G. A., Krelowski J., Biennier L., Beletsky Y., Song I.-O., 2011, *ApJ*, 728, 154
Sephton M. A., 2002, *Natural Product Reports*, 19, 292
Sloan G. C., Hayward T. L., Allamandola L. J., Bregman J. D., DeVito B., Hudgins D. M., 1999, *ApJ*, 513, L65
Sloan G. C., et al., 2007, *ApJ*, 664, 1144
Smith J. D. T., et al., 2007, *ApJ*, 656, 770
Tielens A. G. G. M., 2008, *ARA&A*, 46, 289
Vats A., Pathak A., Onaka T., Buragohain M., Sakon I., Endo I., 2022, *PASJ*, 74, 161
Verstraete L., et al., 2001, *A&A*, 372, 981
Western C. M., 2017, *Journal of Quantitative Spectroscopy and Radiative Transfer*, 186, 221

APPENDIX A: CALCULATED ROTATIONAL SPECTRA AT DIFFERENT TEMPERATURES

This paper has been typeset from a $\text{\TeX}/\text{\LaTeX}$ file prepared by the author.

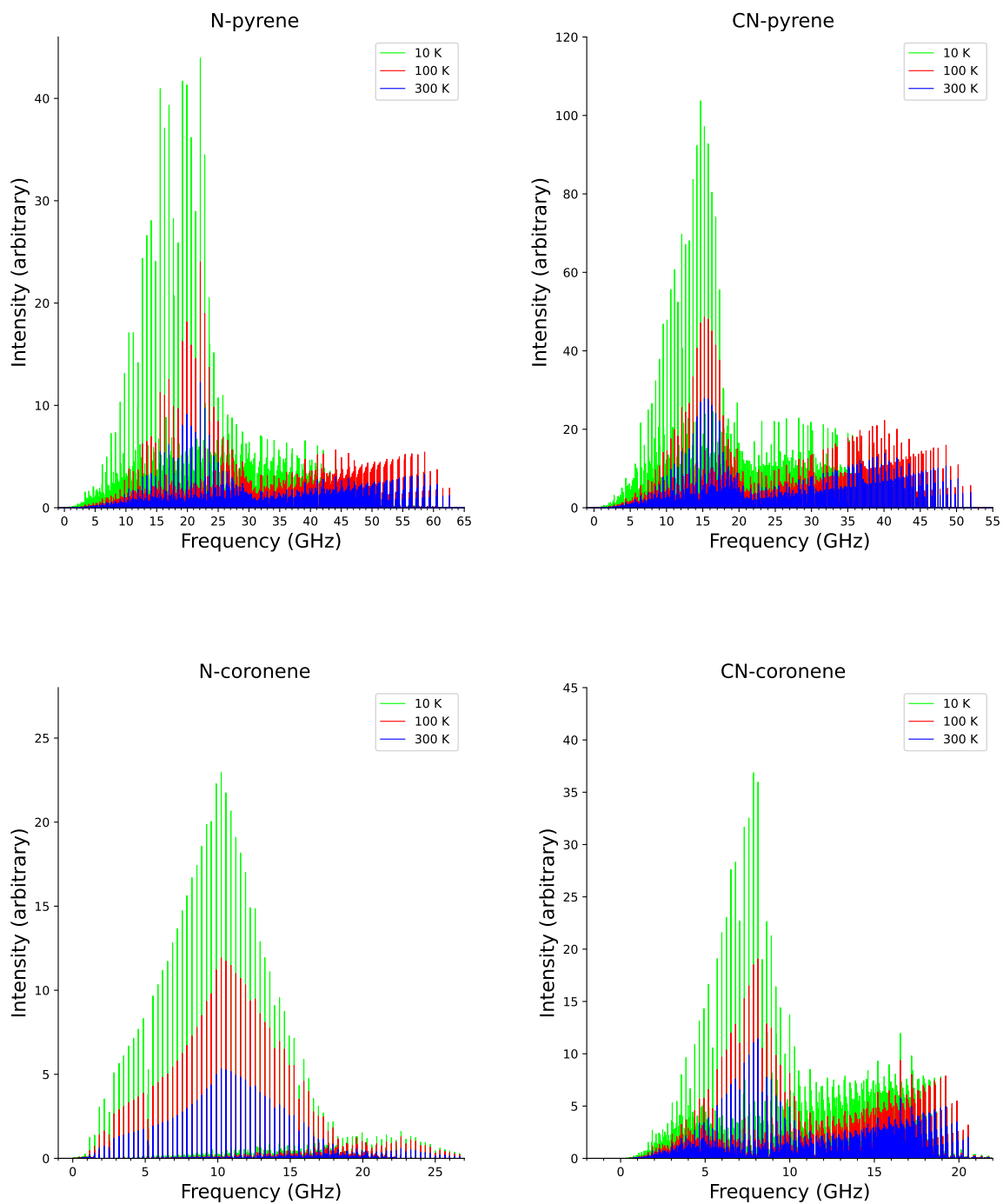


Figure A1. Calculated rotational spectra of the considered N- and CN-PAHs at 10 K (green), 100 K (red) and 300 K (blue).